



Luke Zhao · Feng Jin

The adjustment of electro-elastic properties in non-uniform flexoelectric semiconductor nanofibers

Received: 18 July 2022 / Revised: 9 September 2022 / Accepted: 23 October 2022 / Published online: 22 November 2022
© The Author(s), under exclusive licence to Springer-Verlag GmbH Austria, part of Springer Nature 2022

Abstract To explore the method of adjusting electro-elastic coupling properties in flexoelectric semiconductor nanofibers, the theoretical model is established, and the non-uniform fibers which can adjust the electro-elastic properties are designed. In order to solve the differential equations with variable coefficients in the established model, the differential quadrature method is adopted to approximate the real solutions. Before analysis, the convergence and correctness of the adopted method are investigated systematically. Considering a fiber with linear profile, it is found that the distributions of all field quantities can be adjusted by manipulating the shape of the cross section. The maximum values of all field quantities appear at the narrow end where the stiffness is the minimum in the entire fiber. By investigating the effects of the cross section parameter, flexoelectric coefficient and initial carrier density on the electro-elastic field quantities, it can be observed that the field quantities are sensitive to the variation of these parameters. Besides, studying the charge production indicates that the total charge in the flexoelectric semiconductor is dominated by the polarization charge. In symmetric non-uniform fibers, the potential barriers and wells which are produced by axial tensile load or piecewise loads are studied, respectively. It is revealed that the height of the potential barrier and the depth of the potential well can be adjusted by designing the non-uniform cross section. Furthermore, it is found that the perturbation carrier in a PN junction tends to concentrate in the zone near the narrow position. The studies in this paper could be the guidance for the applications of flexoelectric semiconductor fibers.

1 Introduction

The piezoelectric semiconductor (PS) has attracted much attention in recent years. In PS, the charge carrier is driven by piezoelectric potential, and the electric potential is produced by external load. This kind of coupled characteristic between piezoelectricity and semiconduction in PS belongs to the field of piezotronics [1, 2]. With the development of manufacture technology, various PS structures have been synthesized, such as nanowires, nanobelts or nanodiskettes. [3]. Based on these structures, PS has been successfully used to fabricate many kinds of electric devices, such as nanogenerators [4, 5], sensors [6–8], transistors [9, 10], logic devices [11, 12] and so on.

To reveal the underlying mechanisms of electro-elastic coupling properties, many research works on PS are carried out. Zhang et al. [13, 14] demonstrated the carrier redistribution in ZnO nanofiber systematically and concluded how external load adjusts the electro-elastic fields thoroughly. Based on the mechanism of the interaction between stress and the electrical field quantities in PS, Fan et al. [15] proposed the potential barrier and well in semiconductor can be realized by applying piecewise stresses. Dai [16] and Zhang [17] et al. studied the carrier redistribution when the PS fiber undergoes bending deformation. By applying harmonic

L. Zhao · F. Jin (✉)
State Key Laboratory for Strength and Vibration of Mechanical Structures, School of Aerospace, Xi'an Jiaotong University,
Xi'an 710049, Shaanxi, China
e-mail: jinfengzhao@263.net

loads, Li [18] and Wang [19] et al. studied the forced vibration and revealed the charge carriers tend to reduce the efficiency of energy conversion in PS. When the acoustic waves propagate in PS, Yang [20, 21] and Gu [22] et al. found that the acoustic waves are amplified. Besides, Yang [23], Hu [24], Sladek [25] and Zhao [26] et al. analyzed the cracks in PS. As the element of integrated circuit, PN junction between p-type semiconductor and n-type semiconductor is also studied. Luo [27] and Guo [28] et al. studied the potential barrier and the carrier redistribution, as well as concluded the mechanism of interaction between load and electrical properties in a PS fiber with PN junction. Considering the thermoelasticity and pyroelectricity of ZnO, Cheng et al. [29, 30] studied the thermal induced carrier redistribution in single PS fiber and revealed the electrical and mechanical properties in a fiber with PN junction.

Notably, the functions in PS can also be realized in composite piezoelectric semiconductor structures, such as acoustoelectric effect [31] or acoustoelectric amplification [32]. Significantly, some new conclusions are obtained in composite piezoelectric semiconductor structures. By manipulating the thickness ratio between piezoelectric and semiconductor materials, the carrier distribution is sensitively altered [33, 34]. These studies explored a new approach to adjust the transportation of carriers. Besides, the composite structure which is composed by multiferroic magneto-electric materials and semiconductor is also studied [35, 36]. With magneto-electric coupling effect, the carrier in semiconductor can be driven by external magnetic field. This discovery enriches the method adjusting the carrier transportation. All of the discussions above show that the composite structure has great potential in semiconductor-based devices.

Apart from piezoelectric potential, flexoelectric potential could also be an alternative internal field driving the charge carrier. Zhao [37, 38] et al. analyzed the effects of flexoelectricity and strain gradient on the electrical or mechanical characteristics in PS nanowires. Sun [39] et al. studied the effect of flexoelectricity on piezotronic responses in PS bilayer structure. However, these studies treated the flexoelectricity as a kind of higher-order effect. Recently, the study on silicon [40] proved the existence of flexoelectric coupling in centrosymmetric semiconductors experimentally. And the concept of flexotronics, which concerns the flexoelectric potential-driven carrier transportation [41–44] mainly, is proposed.

However, the small flexoelectric coefficient limits the development of flexoelectric semiconductor (FS). To obtain considerable flexoelectric coupling, a beam with non-uniform cross section can be designed [45, 46]. Ren et al. [47] illustrated the variation of cross section can provide strain gradient. Inspired by this, the electro-elastic coupling properties in a FS fiber with non-uniform cross section are studied in this paper. And the mechanism of the interaction among load, electric potential and carrier will be explored.

Beginning with the basic theory of FS in Sect. 2.1, the theoretical model for a FS fiber with arbitrary cross section is established in Sect. 2.2. To solve the differential equations with variable coefficients, differential quadrature method is adopted to approximate the exact solutions in Sect. 3. In Sect. 4, the influences of cross section parameter, flexoelectric coefficient and initial carrier density on the field quantities are investigated. At the same time, the charge production is discussed. In Sect. 5, the potential barrier and well, which are induced by axial load or piecewise loads in symmetric non-uniform fiber, are studied. Furthermore, the distribution of perturbation carrier density in PN junction is also focused in Sect. 6. As a summary, some conclusions are drawn in Sect. 7.

2 Fundamental equations for flexoelectric semiconductor nanofiber

2.1 Basic theory of flexoelectric semiconductor

In this subsection, the basic theory for FS is reviewed briefly. To depict the electro-elastic coupling behaviors, the coupled field theory was developed. It consists of the equation of motion (Newton's law), the charge equation of electro-static (Gauss's law), and the conservations of charge for holes and electrons (continuity equations). Mathematically, the governing equations are expressed as [41–43]

$$\begin{aligned} T_{ij,j} - \tau_{ijk,jk} &= \rho \ddot{u}_i, \quad D_{i,i} = q(p - n + N_D^+ - N_A^-), \\ J_{i,i}^p &= -q \dot{p}, \quad J_{i,i}^n = q \dot{n}, \end{aligned} \quad (1)$$

where T_{ij} is the stress tensor, τ_{ijk} represents the higher-order stress tensor, and ρ is mass density. u_i and D_i , respectively, stand for the mechanical displacement tensor and electric displacement tensor, and q is the electronic charge. p and n are concentrations of holes and electrons, N_D^+ and N_A^- denote the impurity concentrations of donors and acceptors. J_i^p and J_i^n are hole and electron current densities, respectively. The

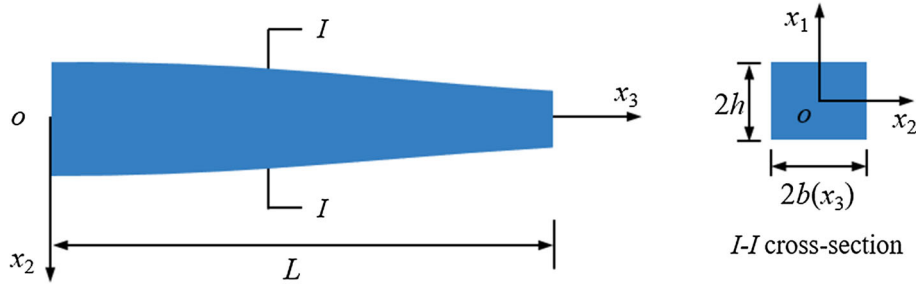


Fig. 1 Sketch of a FS fiber with non-uniform cross section

superscript of dot means a time derivative, and repeated subscripts indicate summation operation. Besides, the corresponding constitutive relations describing material behaviors are given as

$$\begin{aligned} T_{ij} &= c_{ijkl} S_{kl}, \quad \tau_{ijk} = g_{ijklmn} \eta_{lmn} - f_{lijk} E_l, \quad D_i = \varepsilon_{ij} E_j + f_{ijkl} \eta_{jkl}, \\ J_i^p &= qp\mu_{ij}^p E_j - qd_{ij}^p p_{,j}, \quad J_i^n = qn\mu_{ij}^n E_j + qd_{ij}^n n_{,j}, \end{aligned} \quad (2)$$

where c_{ijkl} , g_{ijklmn} , f_{lijk} and ε_{ij} are the elastic constants, higher material constants, flexoelectric constants and dielectric constants, respectively. Referencing to MarkusLazar [48], in order to simplify the higher gradient elasticity and to connect it with the nonlocal isotropic elasticity, the higher-order stress tensors are just simple gradients of the Cauchy-like stress tensor multiplied by two gradient coefficients. Thereby, higher material constants can be approximated by $l_0^2 c_{ijklm} \delta_{kn}$ based on strain gradient theory. Here, l_0 is scale coefficient and δ_{kn} is Kronecker delta. μ_{ij}^p (μ_{ij}^n) and d_{ij}^p (d_{ij}^n) represent the carrier mobility and carrier diffusion constants of holes (electrons). And the strain S_{ij} , electric field E_k and strain gradient η_{jkl} can be expressed by the mechanical displacement u_i and electric potential φ via

$$S_{ij} = \frac{1}{2}(u_{i,j} + u_{j,i}), \quad \eta_{jkl} = S_{jkl,l}, \quad E_k = -\varphi_{,k}. \quad (3)$$

It should be noted that the nonlinear terms are contained in current densities, which cause the difficulty in deriving analytical solutions. For the purpose of simplifying derivation, linearization approach is introduced here, i.e.,

$$p = p_0 + \Delta p, \quad n = n_0 + \Delta n, \quad p_0 = N_A^-, \quad n_0 = N_D^+, \quad (4)$$

where N_A^- and N_D^+ are constants for the uniform impurities, and Δp and Δn are assumed as small perturbation for carrier concentration. With the help of linearization process, (1)₂₋₄ and (2)₄₋₅ can be rewritten as

$$D_{i,i} = q(\Delta p - \Delta n), \quad J_{i,i}^p = -q\Delta \dot{p}, \quad J_{i,i}^n = q\Delta \dot{n}, \quad (5)$$

$$J_i^p \cong qp_0\mu_{ij}^p E_j - qd_{ij}^p \Delta p_{,j}, \quad J_i^n \cong qn_0\mu_{ij}^n E_j + qd_{ij}^n \Delta n_{,j}. \quad (6)$$

The linear and homogeneous equations above can be utilized conveniently to analyze the electro-elastic coupling behaviors in FS within the small deformation assumption. After the geometric model and boundary conditions are given, the multi-field coupling problem can be solved mathematically.

2.2 One-dimensional model for flexoelectric semiconductor nanofiber

A fiber with arbitrary cross section is considered, and the sketch is given in Fig. 1. The fiber has fixed length L along x_3 direction and height $2h$ along x_1 direction. Herein, the width of the fiber is changed symmetrically in the form of $b(x_3)$, where certain function describes corresponding profile. Besides, the material of semiconductor belongs to the class of crystal that is a centrosymmetric cubic (m3m) without the piezoelectric coupling.

Referencing to Fang [49], when a non-uniform fiber is stretched by external load along x_3 direction, the variation of electrical properties in cross section is small and then its influences on the axial results are

tiny. Therefore, the mechanical displacement, electric potential, and carrier concentration perturbation can be approximated by

$$\begin{aligned} u_3(x_1, x_2, x_3, t) &\cong u_3(x_3, t), \quad \varphi(x_1, x_2, x_3, t) \cong \varphi(x_3, t), \quad \Delta p(x_1, x_2, x_3, t) \cong \Delta p(x_3, t), \\ \Delta n(x_1, x_3, t) &\cong \Delta n(x_3, t). \end{aligned} \quad (7)$$

Correspondingly, the relevant strain S_{33} , strain gradient η_{333} and electric field E_3 can be expressed by

$$S_{33} = u_{3,3}, \quad \eta_{333} = u_{3,33}, \quad E_3 = -\varphi_{,3}. \quad (8)$$

And the relevant stress T_{33} , higher-order stress τ_{333} , electric displacement D_3 , and current densities J_3^p and J_3^n are given by

$$\begin{aligned} T_{33} &= c_{33}u_{3,3}, \quad \tau_{333} = l_0^2 c_{33}u_{3,33} + f_{3333}\varphi_{,3}, \quad D_3 = -\varepsilon_{33}\varphi_{,3} + f_{3333}u_{3,33}, \\ J_3^p &= -qp_0\mu_{33}^p\varphi_{,3} - qd_{33}^p\Delta p_{,3}, \quad J_3^n = -qn_0\mu_{33}^n\varphi_{,3} + qd_{33}^n\Delta n_{,3}. \end{aligned} \quad (9)$$

Considering static problem, where the external load is constant, the time derivatives should be vanished. And the one-dimensional governing equations for axial deformation can be obtained, i.e.,

$$\begin{aligned} [c_{33}A(x_3)u_{3,3} - c_{33}l_0^2A(x_3)u_{3,333} - f_{3333}A(x_3)\varphi_{,33}]_{,3} &= 0, \\ [-\varepsilon_{33}A(x_3)\varphi_{,3} + f_{3333}A(x_3)u_{3,33}]_{,3} &= qA(x_3)(\Delta p - \Delta n), \\ [-p_0\mu_{33}^pA(x_3)\varphi_{,3} - d_{33}^pA(x_3)\Delta p_{,3}]_{,3} &= 0, \\ [-n_0\mu_{33}^nA(x_3)\varphi_{,3} + d_{33}^nA(x_3)\Delta n_{,3}]_{,3} &= 0, \end{aligned} \quad (10)$$

where $A(x_3) = 4b(x_3)h$ is the area of cross section. The governing equations can be used to explain the electro-elastic behaviors in FS fiber along axial direction. It can be found that Eq. (10) will degenerate to the governing equation investigating the pure flexoelectric fiber when semiconduction terms are dropped. In this paper, the FS fiber with extension deformation is one-dimensional problem, according to the research works on strain gradient [50], electric field gradient [51] and semiconductor [37], the general boundary conditions can be simplified and described as

$$\begin{aligned} u_3 &= \bar{u}_3 \text{ or } N = T_{33} + \tau_{333,3} = \bar{F}, \quad u_{3,3} = \bar{u}_{3,3} \text{ or } \tau_{333} = \bar{\tau}, \quad \varphi = \bar{\varphi} \text{ or } D_3 = \bar{D}, \\ \Delta p &= \Delta \bar{p} \text{ or } J_3^p = \bar{J}_3^p, \quad \Delta n = \Delta \bar{n} \text{ or } J_3^n = \bar{J}_3^n, \end{aligned}$$

where \bar{u}_3 , \bar{F} , $\bar{u}_{3,3}$, $\bar{\tau}$, $\bar{\varphi}$, \bar{D} , $\Delta \bar{p}(\Delta \bar{n})$ and $\bar{J}_3^p(\bar{J}_3^n)$ are the certain displacement, axial force, displacement gradient, higher-order stress, electric potential, electric displacement, perturbation carrier density and electric current, respectively. For a specific problem, these quantities will be determined to make the solutions of governing equations unique.

3 Extension of a flexoelectric semiconductor nanofiber

3.1 Description of the problem

In this paper, a non-uniform fiber which is stretched by constant load F at two free ends is taken into account, as shown in Fig. 2. Here, considering the boundaries are electrically isolated, i.e., there are no concentrated charges at both ends and no currents flow in or out at the ends. Therefore, the relevant boundary conditions are [37]

$$\begin{aligned} N_3(0) = N_3(L) = F, \quad \tau_{333}(0) = \tau_{333}(L) = 0, \quad D_3(0) = D_3(L) = 0, \\ J_3^p(0) = J_3^p(L) = 0, \quad J_3^n(0) = J_3^n(L) = 0. \end{aligned} \quad (11)$$

It can be found that the electrically isolated conditions at both ends indicate $J_3^p = J_3^n = 0$. In this situation, the subtraction between Eq. (10)₃ and Eq. (10)₄ yields

$$-\left(p_0 \frac{\mu_{33}^p}{d_{33}^p} + n_0 \frac{\mu_{33}^n}{d_{33}^n}\right)\varphi_{,3} = (\Delta p - \Delta n)_{,3} \quad (12)$$

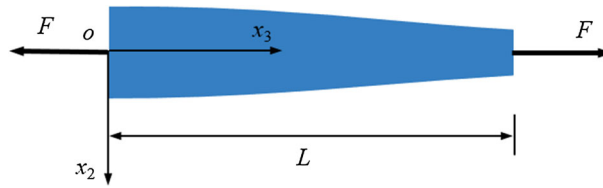


Fig. 2 Sketch for a stretched non-uniform fiber

Significantly, according to the Einstein relation, carrier mobility $\mu_{33}^p(\mu_{33}^n)$ and the carrier diffusion constants $d_{33}^p(d_{33}^n)$ satisfy

$$\frac{\mu_{33}^p}{d_{33}^p} = \frac{\mu_{33}^n}{d_{33}^n} = \frac{q}{k_B T}, \tag{13}$$

where k_B is the Boltzmann constant and T is the absolute temperature. Substituting Eq. (13) into Eq. (12) and integrating the resultant equation leads to

$$\Delta p - \Delta n = -(p_0 + n_0) \frac{q}{k_B T} \varphi + C, \tag{14}$$

where C can be treated as reference value for any point in entire fiber, which does not influence the distribution of electric potential. Here, $C = 0$ is acceptable.

Besides, according to the discussions in Cheng’s studies [30], a reference value for displacement should be given for unique solution. Generally, the reference value is assumed as the displacement at the middle point in a symmetric fiber. Referencing to Zhang [52], the reference value can also be predetermined at one of the ends in the fiber, which does not influence the distributions of displacement, electric potential or the other field quantities. In this paper, we select the left end (i.e., $x_3 = 0$) as reference point. In this condition, $u_3(0) = 0$ replaces $N_3(0) = F$ as a new boundary condition.

Eliminating $\Delta p - \Delta n$, the governing equations are simplified to

$$\begin{aligned} [c_{33}A(x_3)u_{3,3} - c_{33}l_0^2A(x_3)u_{3,333} - f_{3333}A(x_3)\varphi_{,3}]_{,3} &= 0, \\ [-\varepsilon_{33}A(x_3)\varphi_{,3} + f_{3333}A(x_3)u_{3,33}]_{,3} + A(x_3)\frac{q^2(p_0 + n_0)}{k_B T}\varphi &= 0. \end{aligned} \tag{15}$$

Solving Eq. (15), the electro-elastic fields in FS can be analyzed under the boundary conditions. Furthermore, the influences of all parameters on the electro-elastic coupling properties can be revealed.

3.2 Solutions

Obviously, the governing equations are the differential equations with variable coefficients, which are hard to look for analytical solutions. To study the problem that is described in Sect. 3.1, differential quadrature method (DQM) is adopted in this paper [53]. In DQM, a continuous function can be approximated by a linear sum of weighted coefficients and function values at all discrete points. According to the discrete rule of DQM, the unknown displacement u_3 , electric potential φ and the values at j -th point for their k -th derivatives can be expressed by

$$\{u_3(\xi), \varphi(\xi)\} = \sum_{j=1}^N L_j(\xi) \{U_j, \Phi_j\}, \quad \{u_3^{(k)}(\xi_i), \varphi^{(k)}(\xi_i)\} = \sum_{j=1}^N C_{ij}^{(k)} \{U_j, \Phi_j\}, \tag{16}$$

where U_j and Φ_j are the values of u_3 and φ at j th discrete point, $\xi = x_3/L$ is non-dimensional coordinate, $L_j(\xi)$ is Lagrange interpolation polynomials, $C_{ij}^{(k)}$ is k -th weighting coefficient, which is calculated by using recurrence relationship, the subscriptions i and j index the number of discrete points. Notably, the discrete points are selected in the pattern of

$$\xi_j = \frac{1}{2} \left[1 - \cos \frac{(j-1)\pi}{N-1} \right], \quad j = 1, 2, 3, \dots, N. \tag{17}$$

Applying the DQM to Eq. (15) yields algebraic equations respecting u_j and φ_j , i.e.,

$$\begin{aligned}
& \frac{c_{33}}{L} A_{,3}(\xi_i) \sum_{j=1}^N C_{ij}^{(1)} U_j - \frac{c_{33}}{L^3} I_0^2 A_{,3}(\xi_i) \sum_{j=1}^N C_{ij}^{(3)} U_j - \frac{f_{3333}}{L^2} A_{,3}(\xi_i) \sum_{j=1}^N C_{ij}^{(2)} \Phi_j \\
& + \frac{c_{33}}{L^2} A(\xi_i) \sum_{j=1}^N C_{ij}^{(2)} U_j - \frac{c_{33}}{L^4} I_0^2 A(\xi_i) \sum_{j=1}^N C_{ij}^{(4)} U_j - \frac{f_{3333}}{L^3} A(\xi_i) \sum_{j=1}^N C_{ij}^{(3)} \Phi_j = 0, \\
& i = 3, 4, \dots, N-2; j = 1, 2, \dots, N, \\
& - \frac{\varepsilon_{33}}{L} A_{,3}(\xi_i) \sum_{j=1}^N C_{ij}^{(1)} \Phi_j + \frac{f_{3333}}{L^2} A_{,3}(\xi_i) \sum_{j=1}^N C_{ij}^{(2)} U_j - \frac{\varepsilon_{33}}{L^2} A(\xi_i) \sum_{j=1}^N C_{ij}^{(2)} \Phi_j + \\
& \frac{f_{3333}}{L^3} A(\xi_i) \sum_{j=1}^N C_{ij}^{(3)} U_j + A(\xi_i) \frac{q^2(p_0 + n_0)}{k_B T} \Phi_i = 0, \\
& i = 2, 3, \dots, N-1; j = 1, 2, \dots, N.
\end{aligned} \tag{18}$$

In the derivations before, the boundary conditions $J_3^p(0) = J_3^p(L) = J_3^n(0) = J_3^n(L) = 0$ have been considered, which are not discussed later. It should be emphasized that the fiber is treated as electrically neutral for the reference state, the perturbation carrier density must satisfy the global charge neutrality conditions $\int_0^L A \Delta p dx_3 = 0$ and $\int_0^L A \Delta n dx_3 = 0$. Only one of them is independent. For pure p-type or n-type semiconductor, the global charge neutrality condition is satisfied automatically by integrating the Eq. (10)₂ along the length under the electrically isolated boundary conditions. Now, the unsatisfied boundary conditions can be rewritten as

$$\begin{aligned}
& u_3(0) = 0, U_1 = 0, \\
& N_3(L) = F, \frac{c_{33}}{L} A(\xi_N) \sum_{j=1}^N C_{Nj}^{(1)} U_j - \frac{c_{33}}{L^3} I_0^2 A(\xi_N) \sum_{j=1}^N C_{Nj}^{(3)} U_j - \frac{f_{3333}}{L^2} A(\xi_N) \sum_{j=1}^N C_{Nj}^{(2)} \Phi_j = F, \\
& \tau_{333}(0) = 0, \frac{c_{33}}{L^2} I_0^2 \sum_{j=1}^N C_{1j}^{(2)} U_j + \frac{f_{3333}}{L} \sum_{j=1}^N C_{1j}^{(1)} \Phi_j = 0, \\
& \tau_{333}(L) = 0, \frac{c_{33}}{L^2} I_0^2 \sum_{j=1}^N C_{Nj}^{(2)} U_j + \frac{f_{3333}}{L} \sum_{j=1}^N C_{Nj}^{(1)} \Phi_j = 0, \\
& D_3(0) = 0, - \frac{\varepsilon_{33}}{L} \sum_{j=1}^N C_{1j}^{(1)} \Phi_j + \frac{f_{3333}}{L^2} \sum_{j=1}^N C_{1j}^{(2)} U_j = 0, \\
& D_3(L) = 0, - \frac{\varepsilon_{33}}{L} \sum_{j=1}^N C_{Nj}^{(1)} \Phi_j + \frac{f_{3333}}{L^2} \sum_{j=1}^N C_{Nj}^{(2)} U_j = 0, \\
& j = 1, 2, \dots, N.
\end{aligned} \tag{19}$$

Equation (18) and Eq. (19) give a linear algebraic equation system, which can be used to solve the unknown values for displacement and electric potential at discrete points. With the help of derivations above, the differential equations with variable coefficients can be solved conveniently.

4 Electro-elastic fields in non-uniform FS nanofiber

In this section, we consider a p-type semiconductor for numerical analysis. Correspondingly, the initial carrier concentration n_0 and perturbation carrier density Δn are eliminated from the derivations in Sect. 3. Here, a common used FS material Si is selected for numerical calculation. The relevant parameters are [42]

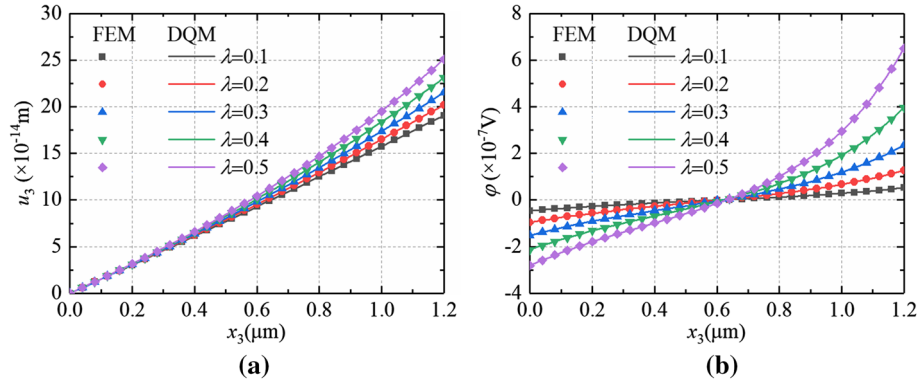


Fig. 3 The comparisons between FEM and DQM. **a** Displacement u_3 ; **b** Electric potential φ

$$c_{33} = 165.7 \text{ GPa}, \quad \varepsilon_{33} = 0.1035 \times 10^{-9} \text{ F/m}, \quad f_{3333} = 1 \times 10^{-9} \text{ C/m}, \quad l_0 = 1 \times 10^{-9} \text{ m},$$

$$p_0 = 1 \times 10^{20} / \text{m}^3, \quad k_B T / q = 0.026 \text{ V}, \quad L = 1200 \text{ nm}, \quad h = 100 \text{ nm}, \quad F = 1 \text{ nN}.$$

In this paper, the variation of the cross section is focused, correspondingly, the variation pattern of the fiber should be given firstly. Reviewing the studies of Ren [47] and Fang [49], the linear profile and quadratic profile could lead to similar results. Consequently, only linear profile is selected as example, i.e., the width of the fiber varies in the form of

$$b(x_3) = B \left(1 - \lambda \frac{x_3}{L} \right), \quad (20)$$

where $B = 100 \text{ nm}$ is the width at left end ($x_3 = 0$) and the parameter λ varies in the range $(0,1)$, which manipulates the shape of the fiber.

4.1 Convergence and validation

Before analysis, a proper number of grid point should be determined, which needs to satisfy the convergence requirement and ensure enough accuracy. After investigating different numbers of grid point, $N = 150$ for DQM provides enough convergence. Besides, to prove the correctness of the results from DQM in this paper, finite element method (FEM) is performed based on COMSOL Multiphysics software. The comparisons between the results from DQM and FEM are given in Fig. 3, where $\lambda = 0.1, 0.2, 0.3, 0.4, 0.5$ are investigated, respectively. It can be observed that the DQM's results coincide well with FEM's results, as a result, the correctness of DQM is proved. In Fig. 4, the comparisons for the displacement and electric potential between linear and nonlinear theories [54] are carried, in which, the description on nonlinear theory can be found in Appendix 1. From the calculated results, it can be found the results from this paper are very close to the nonlinear results. It indicates the derivations in this paper are suitable to explain the underlying mechanisms of flexoelectric semiconductor accurately.

4.2 Effects of λ on the electro-elastic field quantities

To illustrate how the variation of cross section changes the electro-elastic field quantities, Fig. 5 gives the strain gradient η_{333} , electric field E_3 , polarization P_3 and perturbation carrier density Δp . The polarization vector can be calculated through $P_3 = D_3 - \varepsilon_0 E_3$. The perturbation carrier can be obtained based on Eq. (14) by ignoring n_0 and Δn .

In Fig. 5a, it can be seen that the increment of λ increases the strain gradient for entire fiber. At the same time, the strain gradient increases along the axial direction for each given λ . This phenomenon comes from the variation of stiffness. When λ is set in the range $(0,1)$, the stiffness of entire fiber is cut down along axial direction continuously. Especially for right end, the stiffness reaches the minimum value. Therefore, it can be

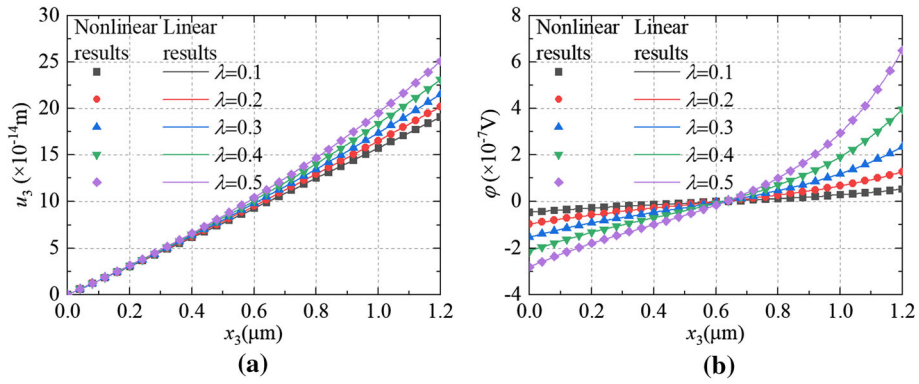


Fig. 4 The comparisons between linear and nonlinear results. **a** Displacement u_3 ; **b** Electric potential φ

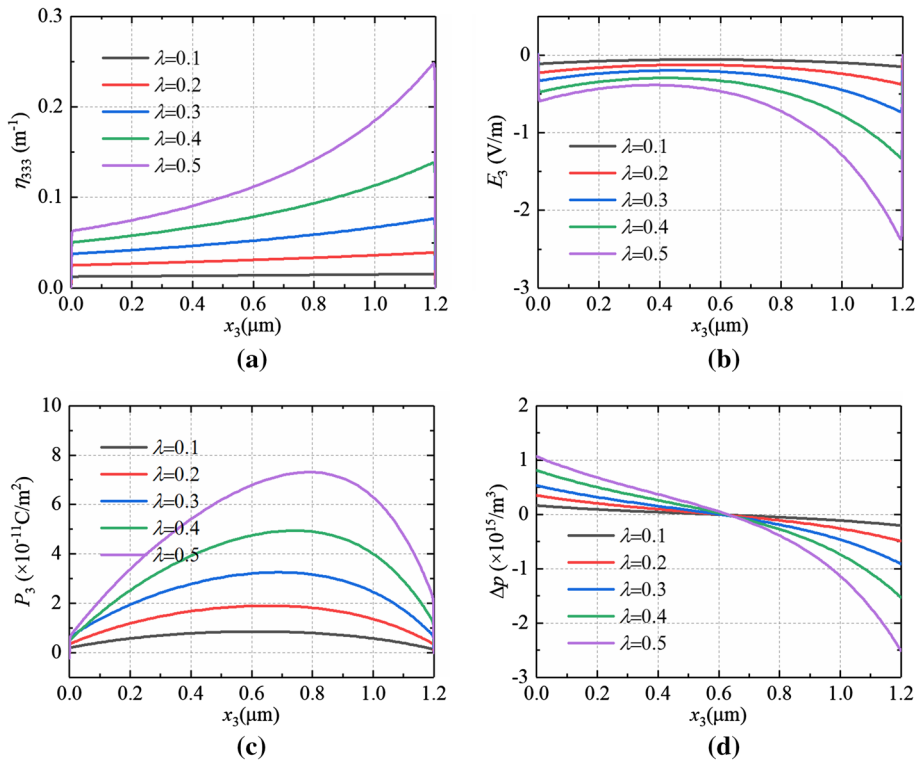


Fig. 5 The effects of λ on the electro-elastic field quantities. **a** Strain gradient; **b** electric field; **c** Polarization; **d** Perturbation carrier density

concluded that a large λ induces large strain gradient. Because of the increased strain gradient, the electric potential difference between two ends in the fiber is also increasing as shown in Fig. 3b. In Fig. 5b and c, electric field and polarization are given, where the absolute values of these two quantities have similar tendency with strain gradient. It indicates the electric field and polarization are closely related to the strain gradient in FS. Driven by internal electric potential, more perturbation carriers are produced and reach the maximum values at the right end. From the calculated results, it can be concluded that the rapid variation of cross section produces large fields and the maximum values of field quantities appear in the zone whose stiffness is minimum in entire fiber. Furthermore, comparing the results for different λ , it can also be concluded that the flexoelectric effect is enhanced by the variation of the cross section.

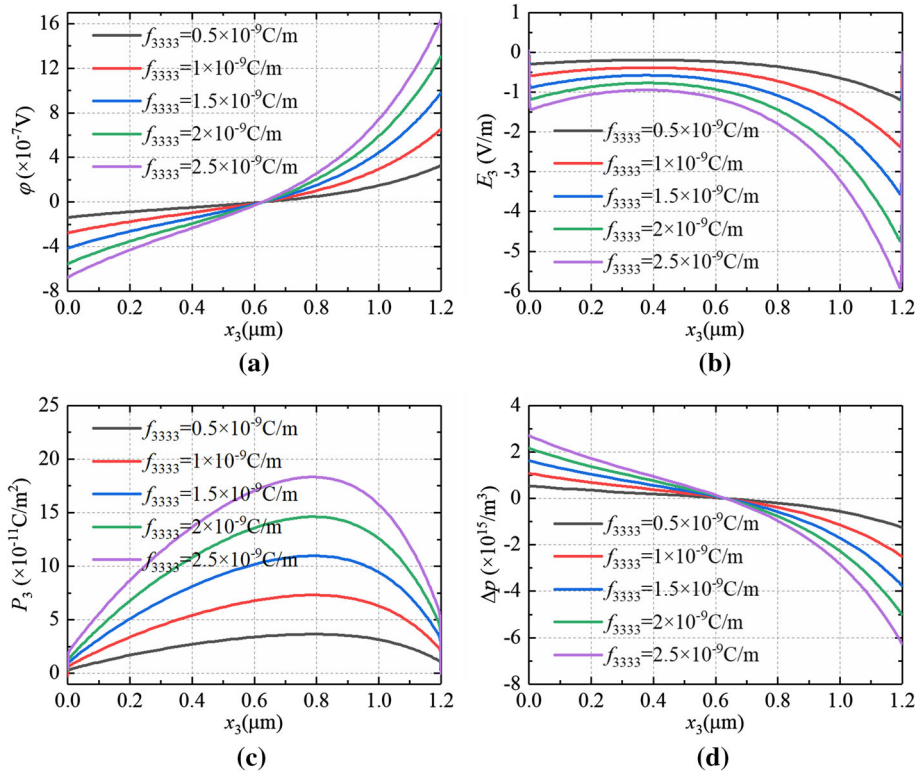


Fig. 6 The effects of f_{3333} on the electro-elastic fields. **a** Electric potential; **b** Electric field; **c** Polarization; **d** Perturbation carrier density

4.3 Effects of f_{3333} on the electrical field quantities

The flexoelectric coefficient f_{3333} is an electrical parameter, which mainly influences the electrical properties. In this section, the effects of f_{3333} on the electric potential, electric field, polarization and perturbation carrier density are focused, as shown in Fig. 6. Cooperating with the non-uniform cross section, all electrical field quantities exhibit the tendency of increment when the flexoelectric coefficient is set from $0.5 \times 10^{-9} \text{C/m}$ to $2.5 \times 10^{-9} \text{C/m}$. Especially, at the narrow end, the increments of field quantities are much faster than them at the broad end. Although a distinct flexoelectric effect can be observed with the help of non-uniform cross section, the values of all field quantities are still relative small in Si. For the purpose of obtaining considerable values of field quantities, another way to further enhance the flexoelectric effect should be explored on the basis of this paper. Or, a new FS material with large flexoelectric coefficient should be found to replace Si. For the purpose of this paper, we can conclude the general tendencies of flexoelectric effect from the calculated results, which provide useful reference data to study similar FS material in the future. In view of this, the study in this paper is still meaningful.

4.4 Effects of p_0 on the electrical field quantities

As a parameter which can be adjusted artificially in experiment or engineering application, the effect of initial carrier density p_0 on the electrical field quantity is not negligible. Figure 7 gives the electrical field quantities for different given initial carrier densities. Because the carrier screening effect, the electric potential and electric field are decreasing, however, the polarization and perturbation carrier density are increasing. It can also be found that the variation is relatively small when the initial carrier density is smaller than $1 \times 10^{19} / \text{m}^3$. On the contrary, the variations in all results become much faster once the initial carrier density is larger than $1 \times 10^{19} / \text{m}^3$. The reason for this phenomenon is because the low concentration doping cannot produce more carriers, while there are not enough free carrier screening the electric potential. For high concentration doping, more carriers are produced and the screening effect becomes stronger.

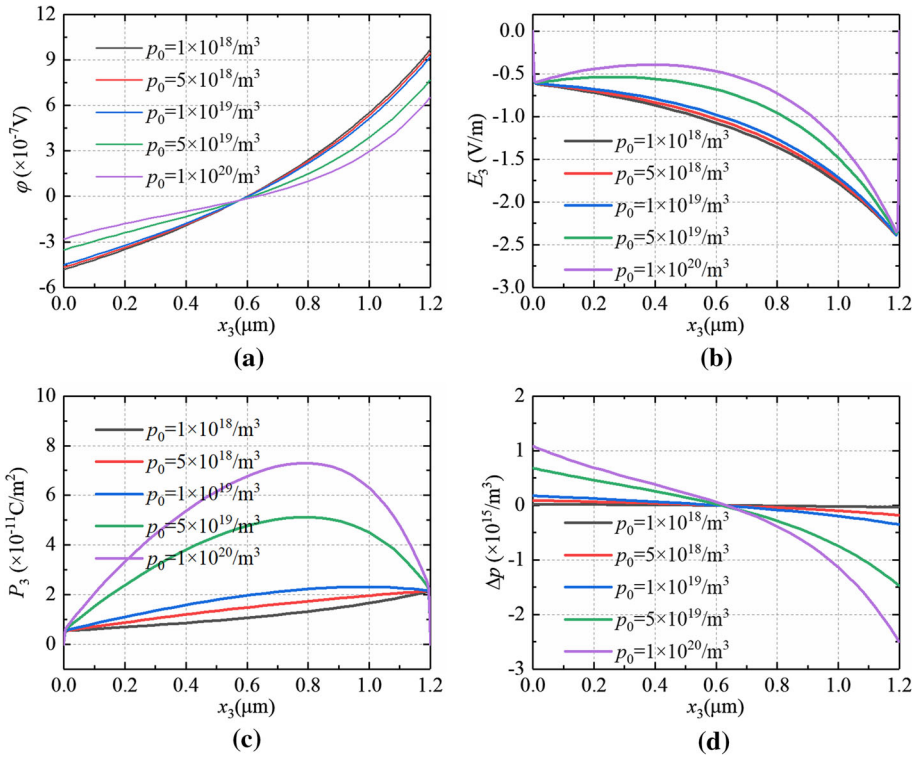


Fig. 7 The effects of p_0 on the electrical field quantities. **a** Electric potential; **b** Electric field; **c** Polarization; **d** Perturbation carrier density

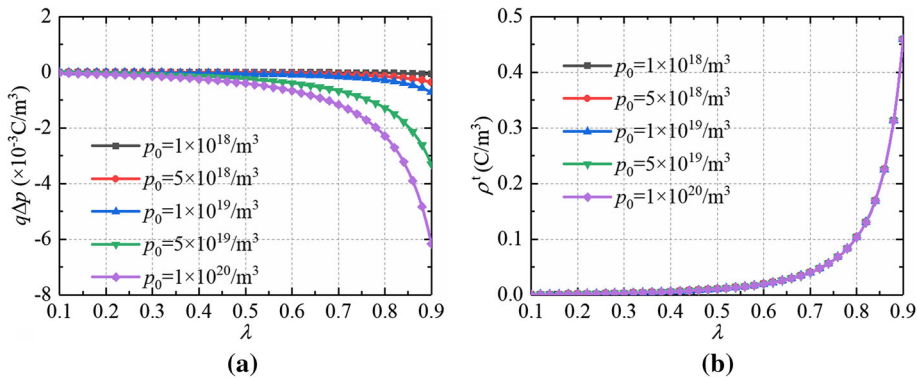


Fig. 8 The charge at the narrow end. **a** Carrier charge; **b** Total charge

4.5 Charges in the non-uniform FS fiber

As a material which can realize the conversion between mechanical load and electrical properties, we prefer to concern the charge production in the fiber. Based on the results above, the expression of carrier charges is $q\Delta p$ and total charge can be calculated through $\rho^t = q\Delta p + \rho^P$. Here, $\rho^P = -P_{3,3}$ is polarization charge. Figure 8 gives the carrier charges and total charges at narrow end for different initial carrier densities when parameter λ varies in the range from 0.1 to 0.9. No matter for carrier charge or for total charge, the values are increasing in the form of approximate exponential rule. It illustrated that the adjustment method manipulating the cross section is feasible. It can be observed that the influence of initial carrier density on carrier charge is distinct. However, there are few influence of initial carrier density on total charge. Besides, the magnitude of total charge is much larger than carrier charge. It indicates that the total charge is dominated by polarization charge.

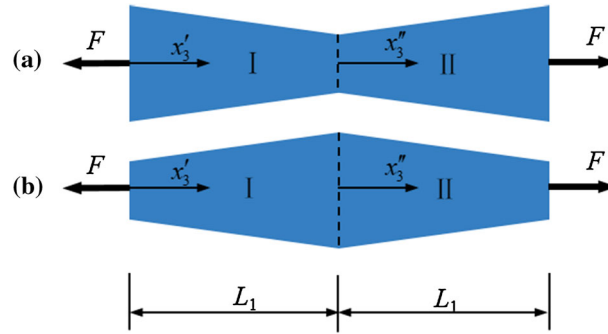


Fig. 9 The sketch of the fiber with axial load

5 Potential barriers and wells in non-uniform FS nanofiber

5.1 The non-uniform fiber under axial load

To further illustrate how non-uniform cross section adjusts electrical properties in FS fiber, two symmetric non-uniform FS fibers are considered in this subsection, as shown in Fig. 9. These two fibers are stretched by a pair of external load at the two ends. Differently, the profile is concave in Fig. 9a and is convex in Fig. 9b. Dividing each fiber into two parts, and setting the local coordinates beginning from the left of each part. The local coordinates are denoted as x'_3 and x''_3 , respectively. The length for each part is L_1 . In the given local coordinates, the widths vary in the form of

$$b = \begin{cases} B\left(1 - \lambda \frac{x'_3}{L_1}\right) & 0 \leq x'_3 < L_1 \\ B\left[1 - \lambda\left(1 - \frac{x''_3}{L_1}\right)\right] & 0 \leq x''_3 \leq L_1 \end{cases} \quad (21)$$

for the fiber with concave profile and

$$b = \begin{cases} B\left[1 - \lambda\left(1 - \frac{x'_3}{L_1}\right)\right] & 0 \leq x'_3 < L_1 \\ B\left(1 - \lambda \frac{x''_3}{L_1}\right) & 0 \leq x''_3 \leq L_1 \end{cases} \quad (22)$$

for the fiber with convex profile.

To describe the electrical properties in the given fibers, the governing equation (i.e., Equation (15)) is still valid for each part. However, the boundary conditions should be reconsidered. For part I, the boundary conditions at left end are

$$N'_3(x'_3 = 0) = F, \tau'_{333}(x'_3 = 0) = 0, D'_3(x'_3 = 0) = 0. \quad (23)$$

For part II, the boundary conditions at right end are

$$N''_3(x''_3 = L_1) = F, \tau''_{333}(x''_3 = L_1) = 0, D''_3(x''_3 = L_1) = 0. \quad (24)$$

At the interface between two parts, the continue conditions should be set, i.e.,

$$\begin{aligned} u'_3(x'_3 = L_1) &= u''_3(x''_3 = 0), N'_3(x'_3 = L_1) = N''_3(x''_3 = 0), \\ u'_{3,3}(x'_3 = L_1) &= u''_{3,3}(x''_3 = 0), \tau'_{333}(x'_3 = L_1) = \tau''_{333}(x''_3 = 0), \\ \varphi'(x'_3 = L_1) &= \varphi''(x''_3 = 0), D'_3(x'_3 = L_1) = D''_3(x''_3 = 0). \end{aligned} \quad (25)$$

Here, in order to fix the reference point for displacement, $N'_3(x'_3 = 0) = F$ is replaced by $u'_3(x'_3 = 0) = 0$ again. Applying the DQM to solve the governing equations under the given boundary conditions and continuity conditions for two parts, the solutions can be obtained. In the following studies, $L_1 = 600 \text{ nm}$ is assumed. In this subsection, we prefer to concern the distribution of electric potential. Figure 10a and b give the electric potentials for the fiber with concave profile and convex profile in global coordinate, respectively. It can be observed that the electric potential is symmetric respects to $x_3 = 0.6\mu\text{m}$, which is quite different from the

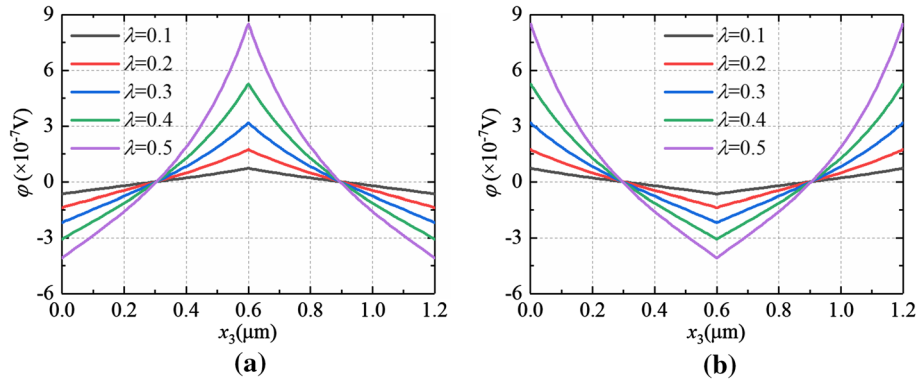


Fig. 10 The distributions of electric potential in non-uniform fiber. **a** In the fiber with concave profile; **b** In the fiber with convex profile

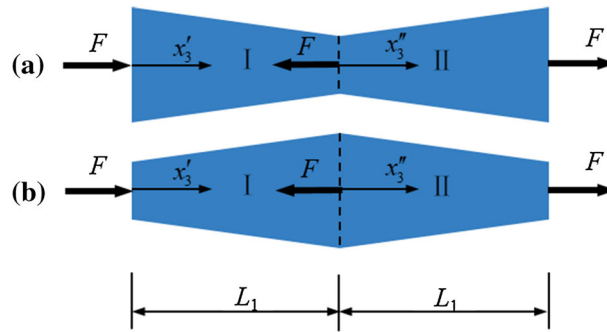


Fig. 11 The sketch of a fiber with piecewise loads

pattern in piezoelectric semiconductor [49]. There are potential barriers and potential wells in the non-uniform fibers. They prevent the mobile charge, whose initial velocity or kinetic energy is not large enough, traveling through the fiber. This phenomenon can be explained from the view of mathematics. The different distributions between FS fiber and PS fiber in symmetric structure are because the derivative of electric potential for FS is one order higher than it for PS fiber in the established model. It can also be explained that the electric potential is induced by the strain gradient, therefore, a symmetric strain gradient produces symmetric electric potential. In addition, it can be found that the potential barrier and well can be adjusted by manipulating the shape of cross section. With the increasing of parameter λ , the higher potential barrier and deeper potential well can be set as shown in Fig. 10.

5.2 The non-uniform fiber with piecewise loads

Referencing to Fan et al. [15], the potential barrier or well can be induced by piecewise stresses. Inspired by this, we consider two fibers with piecewise loads, as shown in Fig. 11, where the part I is compressed and the part II is stretched. Comparing to Fig. 10, the electric potential exhibits quite different distribution rule along the axial direction, as shown in Fig. 12. In the same fiber, the potential barrier and well appear at the two sides of middle point because of the asymmetric strain gradient. With the increasing of parameter λ , the electric potential difference is getting larger at the middle position in the fiber with concave profile. However, for the fiber with convex profile, the electric potential difference is changed distinctly at both ends. These phenomena confirm the conclusion that the maximum values of field quantities appear at the zone whose stiffness is minimum in entire fiber again.

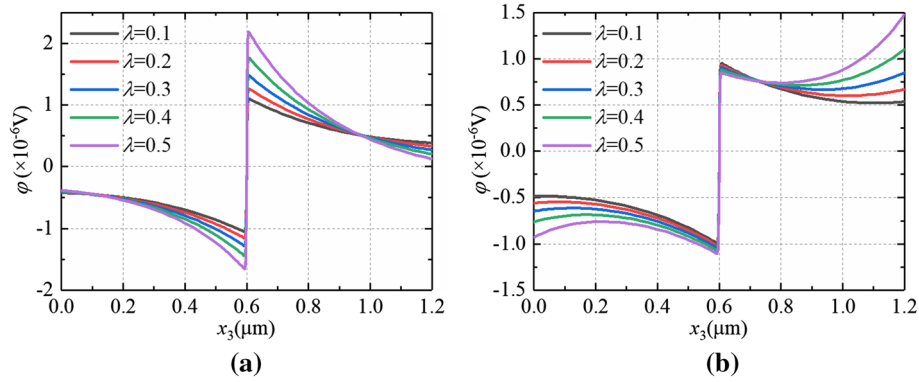


Fig. 12 The distributions of electric potential under piecewise loads. **a** In the fiber with concave profile; **b** In the fiber with convex profile

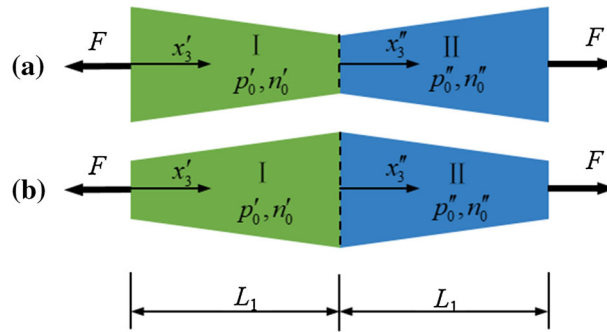


Fig. 13 The sketch of PN junction between two non-uniform FS fibers

6 Carrier redistribution in non-uniform PN junction

In the studies above, only p-type semiconductor is investigated. In this section, a PN junction which subjects to axial load is considered, as shown in Fig. 13. For part I, the initial carrier density for hole (electron) is denoted as p'_0 (n'_0). In part II, the initial carrier density for hole (electron) is denoted as p''_0 (n''_0). Here, $p'_0 = n''_0 = 0.8 \times 10^{20}/m^3$ and $n'_0 = p''_0 = 0.2 \times 10^{20}/m^3$ are assumed. When Eq. (15) is adopted, it can be found the distribution of electric potential in this section is same to it in Fig. 10, therefore, only the distribution of perturbation carrier density is focused here. Figure 14 gives the distributions of perturbation carrier density for the fibers with concave profile and convex profile, respectively. Because of the different initial carrier densities in two parts, no matter for holes or electrons, there are jumps at the interface for perturbation carrier density.

For the same fiber, the distribution pattern for Δp is opposite to Δn . For holes, the majority perturbation carriers exist in the part I. On the contrary, the majority perturbation carriers exist in the part II for electrons. Comparing two kinds of fibers, the majority perturbation carriers appear in the zone near the middle position for a fiber with concave profile. Differently, in the fiber with convex profile, the majority perturbation carriers appear in the zone near the narrow sides. The calculated results indicate that the perturbation carrier density near the interface can be conveniently adjusted by manipulating the shape of cross section to satisfy the requirements in experiment or engineering application.

7 Conclusions

Based on the flexoelectric semiconductor theory, the theoretical model for non-uniform fiber is established. The DQM is introduced to solve the governing equations with variable coefficients and reveal the mechanism how non-uniform cross section adjusts the electro-elastic properties in the FS fibers. Before analysis, the 150 grid points are determined for DQM to ensure enough accuracy. Comparing with the results which are calculated by FEM, the correctness of DQM is proved.

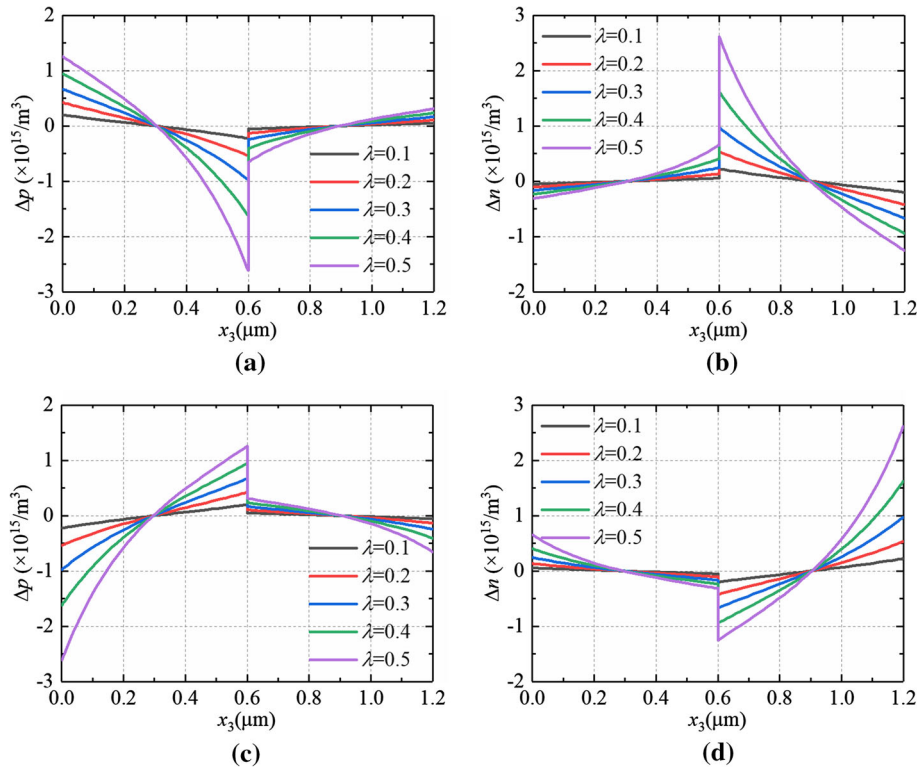


Fig. 14 The distributions of perturbation carrier densities. **a** Δp in the fiber with concave profile; **b** Δn in the fiber with concave profile; **c** Δp in the fiber with convex profile; **d** Δn in the fiber with convex profile

In p-type non-uniform FS fiber, the large electro-elastic field quantities can be produced by a quick variation of cross section along the axial direction. Especially, near the narrow ends, all quantities reach the maximum values. To reveal the underlying mechanisms of FS fiber, the influences of cross section parameter, flexoelectric coefficient and initial carrier density on the electrical properties are investigated. It is found that the electrical properties are sensitive to these parameters. Besides, the investigation about charge production indicates the total charge in the narrow end is dominated by polarization charge. To further illustrate the generality of the theoretical model and DQM, two kinds of fibers with concave and convex profiles are investigated, respectively. Stretched by axial load, there are potential barrier and potential well in the fibers with concave profile and convex profiles, respectively. From the view of mathematics and physics, the reason for this phenomenon is explained in detail. In addition, when the fibers subject to piecewise loads, it is found that the distributions of electric potential are asymmetric. In the end, we investigated the carrier redistribution in non-uniform fibers with PN junction. The calculated results indicate that the distribution of perturbation carrier density can be conveniently adjusted by manipulating the shape of cross section according to the requirements of applications.

In this paper, only the approach manipulating the cross section is adopted to adjust the electro-elastic properties. In the future, the functionally graded fiber or non-uniform composite fiber can also be the objects to study. In these studies, the DQM is still valid to deal with the relevant mathematical models. After surveying the performances which are adjusted by different approaches, the mechanisms of the interaction between mechanical and electrical properties in FS can be revealed thoroughly. These studies might be the guidance for the applications of FS material or the manufacture of smart devices.

Acknowledgements This research is funded by the National Natural Science Foundation of China (Grant No. 12072253).

Declarations

Conflict of interest The authors have no competing interests to declare that are relevant to the content of this paper.

Appendix 1

In this appendix, the exact solution based on nonlinear theory is introduced briefly. According to the relevant literature works [54], the nonlinear equations for p-type semiconductor are expressed by

$$\begin{aligned} [c_{33}A(x_3)u_{3,3} - c_{33}l_0^2A(x_3)u_{3,333} - f_{3333}A(x_3)\varphi_{,33}]_{,3} &= 0, \\ [-\varepsilon_{33}A(x_3)\varphi_{,3} + f_{3333}A(x_3)u_{3,33}]_{,3} &= qA(x_3)(p - N_A^-), \end{aligned} \quad (26)$$

where $p = p_0 \exp(-\frac{q}{k_B T} \varphi)$ can be obtained when the boundaries are electrically isolated, i.e., $J_3^p(0) = J_3^p(L) = 0$. Besides, $p_0 = N_A^-$ is assumed. Solving the governing equations under the given boundary conditions (Eq. (11)) by using COMSOL Multiphysics software, the nonlinear results will be obtained.

References

1. Wang, Z.L.: Piezopotential gated nanowire devices: piezotronics and piezo-phototronics. *Nano Today* **5**, 540–552 (2010)
2. Wu, W., Wang, Z.L.: Piezotronics and piezo-phototronics for adaptive electronics and optoelectronics. *Nat. Rev. Mater.* **1**, 23–24 (2016)
3. Wang, Z.L.: Nanobelts, nanowires, and nanodiskettes of semiconducting oxides—from materials to nanodevices. *Adv. Mater.* **15**, 432–436 (2003)
4. Wang, Z.L.: Piezoelectric nanogenerators based on zinc oxide nanowire arrays. *Science* **312**, 242–246 (2006)
5. Kaur, J., Singh, H.: Fabrication and analysis of piezoelectricity in 0D, 1D and 2D Zinc Oxide nanostructures. *Ceram. Int.* **46**, 19401–19407 (2020)
6. Wang, W., Peng, D., Zhang, H., Yang, X., Pan, C.: Mechanically induced strong red emission in samarium ions doped piezoelectric semiconductor CaZnOS for dynamic pressure sensing and imaging. *Opt. Commun.* **395**, 24–28 (2017)
7. Huolin, H., Hui, Z., Yaqing, C., et al.: High-temperature three-dimensional GaN-based hall sensors for magnetic field detection. *J. Phys. D-Appl. Phys.* **54**, 075003 (2021)
8. Lee, J.W., Ye, B.U., Wang, Z.L., Lee, J.L., Baik, J.M.: Highly-sensitive and highly-correlative flexible motion sensors based on asymmetric piezotronic effect. *Nano Energy* **51**, 185–191 (2018)
9. Han, W., Zhou, Y., Zhang, Y., et al.: Strain-gated piezotronic transistors based on vertical zinc oxide nanowires. *ACS Nano* **6**, 5736 (2012)
10. Wang, X., Zhou, J., Song, J., et al.: Piezoelectric field effect transistor and nanoforce sensor based on a single ZnO nanowire. *Nano Lett.* **6**, 2768–2772 (2006)
11. Yu, R., Wu, W., Ding, Y., et al.: GaN nanobelt-based strain-gated piezotronic logic devices and computation. *ACS Nano* **7**, 6403 (2013)
12. Wu, W., Wei, Y., Wang, Z.L.: Strain-gated piezotronic logic nanodevices. *Adv. Mater.* **22**, 4711–4715 (2010)
13. Zhang, C., Wang, X., Chen, W., et al.: An analysis of the extension of a ZnO piezoelectric semiconductor nanofiber under an axial force. *Smart Mater. Struct.* **26**, 025030 (2017)
14. Zhang, C.L., Wang, X.Y., Chen, W.Q., et al.: Carrier distribution and electromechanical fields in a free piezoelectric semiconductor rod. *J. Zhejiang Univ.-SCI A* **17**, 37–44 (2016)
15. Fan, S., Yuantai, H., Yang, J., et al.: Stress-induced potential barriers and charge distributions in a piezoelectric semiconductor nanofiber. *Appl. Math. Mech.-Engl. Ed.* **40**, 591–600 (2019)
16. Dai, X., Zhu, F., Qian, Z., et al.: Electric potential and carrier distribution in a piezoelectric semiconductor nanowire in time-harmonic bending vibration. *Nano Energy* **43**, 22–28 (2017)
17. Zhang, C., Wang, X., Chen, W., et al.: Bending of a cantilever piezoelectric semiconductor fiber under an end force Generalized Models and Non-classical Approaches in Complex Materials 2, pp. 261–278. Springer, Cham (2018)
18. Li, P., Jin, F., Yang, J.: Effects of semiconduction on electromechanical energy conversion in piezoelectrics. *Smart Mater. Struct.* **24**, 025021 (2015)
19. Guolin, W., Jinxi, L., Xianglin, L., et al.: Extensional vibration characteristics and screening of polarization charges in a ZnO piezoelectric semiconductor nanofiber. *J. Appl. Phys.* **124**, 094502 (2018)
20. Yang, J.S., Yang, X.M., Turner, J.A.: Amplification of acoustic waves in piezoelectric semiconductor plates *Arch. Appl. Mech.* **74**, 288–298 (2004)
21. Yang, J., Yang, X., Turner, J.A.: Amplification of acoustic waves in piezoelectric semiconductor shells. *J. Intell. Mater. Syst. Struct.* **16**, 613–621 (2005)
22. Gu, C., Jin, F.: Shear-horizontal surface waves in a half-space of piezoelectric semiconductors *Philos. Mag. Lett.* **95**, 92–100 (2015)
23. Yang, J.: An anti-plane crack in a piezoelectric semiconductor. *Int. J. Fract.* **136**, L27–L32 (2005)
24. Hu, Y., Zeng, Y., Yang, J., et al.: A mode III crack in a piezoelectric semiconductor of crystals with 6 mm symmetry. *Int. J. Solids Struct.* **44**, 3928–3938 (2007)
25. Sladek, J., Sladek, V., Pan, E., et al.: Dynamic anti-plane crack analysis in functional graded piezoelectric semiconductor crystals. *CMES-Comp. Model. Eng. Sci.* **99**, 273–296 (2014)
26. Zhao, M., Pan, Y., et al.: Extended displacement discontinuity method for analysis of cracks in 2D piezoelectric semiconductors. *Int. J. Solids Struct.* **94**, 50–59 (2016)
27. Luo, Y., Cheng, R., Zhang, C., et al.: Electromechanical fields near a circular PN junction between two piezoelectric semiconductors. *Acta Mech. Solida Sin.* **31**, 127–140 (2018)

28. Guo, M., Li, Y., Qin, G., et al.: Nonlinear solutions of PN junctions of piezoelectric semiconductors. *Acta Mech.* **230**, 1825–1841 (2019)
29. Cheng, R., Zhang, C., Yang, J., et al.: Thermally induced carrier distribution in a piezoelectric semiconductor fiber. *J. Electron. Mater.* **48**, 4939–4946 (2019)
30. Cheng, R., Zhang, C., Chen, W., et al.: Temperature effects on PN junctions in piezoelectric semiconductor fibers with thermoelastic and pyroelectric couplings. *J. Electron. Mater.* **49**, 3140–3148 (2020)
31. Sharma, J.N., Sharma, K.K.: Kumar: Modelling of acoustodiffusive surface waves in piezoelectric-semiconductor composite structure. *J. Mech. Mater. Struct.* **6**, 791–812 (2011)
32. Yang, J.S., Zhou, H.G.: Acoustoelectric amplification of piezoelectric surface waves. *Acta Mech.* **172**, 113–122 (2004)
33. Cheng, R., Zhang, C., Chen, W., et al.: Piezotronic effects in the extension of a composite fiber of piezoelectric dielectrics and nonpiezoelectric semiconductors. *J. Appl. Phys.* **124**, 064506 (2018)
34. Luo, Y., Zhang, C., Chen, W., et al.: Piezopotential in a bended composite fiber made of a semiconductive core and of two piezoelectric layers with opposite polarities. *Nano Energy* **54**, 341–348 (2018)
35. Cheng, R., Zhang, C., Zhang, C., et al.: Magnetically controllable piezotronic responses in a composite semiconductor fiber with multiferroic coupling effects. *Phys. Status Solidi A-Appl. Res.* **217**, 2070012 (2020)
36. Wang, G., Liu, J., Feng, W., et al.: Magnetically induced carrier distribution in a composite rod of piezoelectric semiconductors and piezomagnetics. *Materials* **13**, 3115 (2020)
37. Zhao, MingHao, Liu, X., Fan, CuiYing, et al.: Theoretical analysis on the extension of a piezoelectric semiconductor nanowire: effects of flexoelectricity and strain gradient. *J. Appl. Phys.* **127**, 085707 (2020)
38. Zhao, M., Niu, J., Lu, C., et al.: Effects of flexoelectricity and strain gradient on bending vibration characteristics of piezoelectric semiconductor nanowires. *J. Appl. Phys.* **129**, 164301 (2021)
39. Sun, L., Zhang, Z., Gao, C., et al.: Effect of flexoelectricity on piezotronic responses of a piezoelectric semiconductor bilayer. *J. Appl. Phys.* **129**, 244102 (2021)
40. Wang, L., Liu, S., Feng, X., et al.: Flexoelectronics of centrosymmetric semiconductors. *Nat. Nanotechnol.* **15**, 661–667 (2020)
41. Qu, Y., Jin, F., Yang, J.: Effects of mechanical fields on mobile charges in a composite beam of flexoelectric dielectrics and semiconductors. *J. Appl. Phys.* **127**, 194502 (2020)
42. Qu, Y., Jin, F., Yang, J.: Magnetically induced charge redistribution in the bending of a composite beam with flexoelectric semiconductor and piezomagnetic dielectric layers. *J. Appl. Phys.* **129**, 064503 (2021)
43. Qu, Y., Jin, F., Yang, J.: Torsion of a flexoelectric semiconductor rod with a rectangular cross section. *Arch. Appl. Mech.* **91**, 2027–2038 (2021)
44. Chu, L., Dui, G., Mei, H., et al.: An analysis of flexoelectric coupling associated electroelastic fields in functionally graded semiconductor nanobeams. *J. Appl. Phys.* **130**, 115701 (2021)
45. Yao D, Zhou H, Wang X Y: Characterization method of flexoelectric coefficient of piezoelectrics at nanoscale. In: Symposium on Piezoelectricity, Acoustic Waves, and Device Applications 325–330 2017
46. Zhu, W., Fu, J.Y., Nan, L., et al.: Piezoelectric composite based on the enhanced flexoelectric effects. *Appl. Phys. Lett.* **89**, 2920 (2006)
47. Ren, C., Wang, K.F., Wang, B.L., et al.: Adjusting the electromechanical coupling behaviors of piezoelectric semiconductor nanowires via strain gradient and flexoelectric effects. *J. Appl. Phys.* **128**, 215701 (2020)
48. Lazar, M., Maugin, G.A., Aifantis, E.C.: Dislocations in second strain gradient elasticity. *Int. J. Solids Struct.* **43**, 1787–1817 (2006)
49. Fang, K., Li, P., Li, N., Liu, D., Qian, Z., Kolesov, V., et al.: Model and performance analysis of non-uniform piezoelectric semiconductor nanofibers. *Appl. Math. Model.* **104**, 628–643 (2021)
50. Mindlin, R.D., Eshel, N.N.: On first strain-gradient theories in linear elasticity. *Int. J. Solids Struct.* **4**, 109–124 (1968)
51. Hu, S., Shen, S.: Electric field gradient theory with surface effect for nano-dielectrics. *CMC-Comput. Mat. Contin.* **13**, 63–87 (2009)
52. Zhang, C.L., Luo, Y.X., Cheng, R.R., Wang, X.Y.: Electromechanical fields in piezoelectric semiconductor nanofibers under an axial force. *MRS Adv.* **2**(56), 3421–3426 (2017). <https://doi.org/10.1557/adv.2017.301>
53. Bert, C.W., Malik, M.: Differential quadrature method in computational mechanics: a review. *Appl. Mech. Rev.* **49**, 1–28 (1996)
54. Yang, W., Yuantai, Hu., Pan, E.: Tuning electronic energy band in a piezoelectric semiconductor rod via mechanical loading. *Nano Energy* **66**, 104147 (2019)

Publisher's Note Springer Nature remains neutral with regard to jurisdictional claims in published maps and institutional affiliations.

Springer Nature or its licensor (e.g. a society or other partner) holds exclusive rights to this article under a publishing agreement with the author(s) or other rightsholder(s); author self-archiving of the accepted manuscript version of this article is solely governed by the terms of such publishing agreement and applicable law.